Effect of interatomic potential on simulated grain-boundary and bulk diffusion: A molecular-dynamics study

S. J. Plimpton* and E. D. Wolf

*Semiconductor Research Corporation Program on Microscience and Technology
and School of Applied and Engineering Physics, Cornell University, Ithaca, New York 14853*
(Received 21 July 1989)

Molecular-dynamics methods are used to model diffusion in a $\Sigma = 5$ [100] Al tilt boundary and in bulk. The diffusion coefficient D and activation energy Q for atoms in the boundary and in bulk are calculated for several different Al empirical interatomic pair potentials. These include a Morse potential, spline potentials fitted to bulk experimental data (elastic constants, phonon spectra, etc.), and a pseudopotential. Reasonable agreement is obtained with experimental diffusion values for Al, although activation energies are low. There is also a wide variation in results from one potential to another because the atomic motion is sensitive to the shape of the primary well or minimum of the interatomic potential. Rescaling the data with rough estimates of the different bulk melting temperatures that each potential predicts reduces the discrepancy between potentials. This is shown to be true for virtually any pair potential by calculating diffusion rates for Morse potentials with changing potential-well depth, position, and width. The variations between potentials are also explained in a quantitative sense by a simple calculation of potential-energy-barrier height for vacancy migration in a bulk model. A method is given for using a linear relation between barrier height and melting temperature to predict diffusion coefficients and general transport properties in grain boundaries and bulk for any pair potential in any fcc metal.

I. INTRODUCTION

With the advent of faster computers in recent years, many researchers have used the techniques of molecular dynamics to simulate dynamic grain-boundary behavior. This involves constructing a geometric model of the boundary composed of several hundred to a few thousand atoms and then following the trajectories of the atoms in time as the simulation progresses. Studies have simulated vacancy-diffusion mechanisms in α-Fe and Al boundaries,[1,2] premelting grain-boundary phase transitions,[3-5] grain-boundary sliding and migration,[6] segregation energies of impurities at boundaries,[7] and crack growth at boundaries due to applied stress.[8,9]

The common element in all work of this type is that to perform a molecular-dynamics simulation a potential-energy functional for the system is chosen, which, in turn, determines the force acting on individual atoms. For ease of calculation, this is often a pair potential (as in Refs. 1–8), so that the total force acting on an atom at any instant is simply the sum of all pairwise interactions between the atom and its near neighbors. The time-consuming part of the simulation is integrating Newton's equations of motion for the system, which requires knowing which atoms are close enough neighbors to a particular atom to interact with it. All the physics of such a model is determined by the choice of energy functional or pair potential, since after atom positions and velocities are initialized, the resulting trajectories of the atoms in time are deterministic.

For metals, a great variety of both theoretical and experimentally determined pair potentials exist in the litera-

ture. How the shapes of various potential functions (and hence the force of interaction between atoms) influence the simulated system is not always clear, since some potentials have many minima and inflection points. For example, a molecular-statics grain-boundary simulation uses the potential function to minimize the energy of the boundary and thus find its 0-K structure. Yet, even for these calculations, which do not take dynamic properties into account, the energy and structure of [100] twist boundaries in Al (Ref. 10) and Au (Ref. 11) were found to depend strongly on the choice of pair potential. Similarly, in a review of grain-boundary melting studies, Pontikis[12] noted that the conflicting results of different simulations are due in part to the sensitivity of melting phenomena on the choice of pair potential and cutoff radius for interactions with near neighbors.

In this paper we present a systematic study of how different pair potentials affect the dynamic properties of atoms in a grain boundary by calculating the diffusion coefficient D and activation energy Q in a bicrystal model of a $\Sigma = 5$ (013) tilt boundary for four Al pair potentials. For comparison purposes, in addition to the bicrystal, a bulk model is also simulated. We have focused our efforts on understanding the dynamics of tilt boundaries in Al because of the semiconductor industry's interest in thin-film metallizations subject to diffusion-related reliability problems (i.e., electromigration where tilt boundaries act as fast-diffusion paths for migrating Al atoms), but the results can be extended to any fcc system. Since D and Q are fundamental measures of the relative freedom of atoms in a boundary to move about, the results should also have relevance to more macroscopic effects

such as the crack propagation or boundary sliding and migration mentioned previously, insofar as they can be modeled accurately with pair potentials.

However, it should be noted that the pair-potential approximation for fcc metals, though widely used, is not as complete as density-functional techniques such as the embedded-atom method (EAM) of Daw and Baskes,[13] where the energy of an atom is a function of both a pair-potential term and the electron density due to all other atoms in the model. As derived by Foiles,[14] the EAM energy can be approximated as a single effective pair potential by expanding the embedding functional in a Taylor series and dropping three-body and higher-order terms. The resulting pair potentials for several metals were shown by Foiles to model liquid-metal properties well, and are similar in shape to the Al pair potentials that will be used in the following sections. However, the fuller EAM description of the energy (which includes many-body effects) is known to be more accurate for surfaces (and grain boundaries) where the symmetry of the bulk lattice is lost. While we are not aware of any molecular-dynamics simulations using the EAM that have studied diffusive motion at grain boundaries, it would be fruitful to compare the results of such calculations to those in this paper.

In Sec. II the details of our model and calculations are outlined. This is followed in Sec. III by diffusion results for several pair potentials and an analysis of the factors that contribute to the observed differences. It was found that rescaling the diffusion values by the melting temperature of a simulated bulk model provided the most useful correlation between potentials. In Sec. IV, to further test this dependence, parameters in a simple Al Morse potential are varied and melting temperatures and diffusion rates again calculated. Finally, the simulation melting temperatures are coupled to simple calculations of the potential-energy barrier height for vacancy migration in the bulk to give a method for predicting D and Q in fcc metals for any interatomic pair potential.

II. MODEL AND CALCULATIONS

The basic method for performing a molecular-dynamics simulation on an atomic solid is well known. A small number of atoms (usually a few thousand at most) are placed in a startng configuration that represents the system being modeled. Appropriate border conditions for the simulation box are chosen, as well as an energy functional that describes the total energy of the system as a function of individual atomic positions. Then the energy of the ensemble of atoms is minimized (a molecular-statics calculation) to find a relaxed 0-K equilibrium position for each atom. The molecular-dynamics portion of the simulation is performed by giving each atom a random velocity and integrating Newton's equations of motion for the system of atoms. The output of the simulation is the trajectories in time of each atom, from which various dynamic quantities of interest can be calculated. Within this framework, two models, one for bulk and one for a grain boundary, were simulated.

For a bulk model the starting positions for the Al

atoms are simply the fcc lattice sites. We modeled a cube $5a_0$ on a side ($a_0 = 4.04$ Å in Al), containing 500 atoms, and periodic in all three directions. Simulations for larger bulk models gave similar results.

For a symmetric grain boundary, the first-order approximation for the starting-atom locations are the lattice sites of the appropriate coincidence-site-lattice (CSL) model. We chose to simulate the frequently cited $\Sigma = 5$ (013) boundary, which has a tilt angle of $\theta = 36.9°$. A representation of the model is shown in Fig. 1, where the tilt axis is along the x direction. The model is periodic in the x and y directions, but has a wall of atoms held fixed on either end in the z direction, analogous to the bicrystal model of Kwok, Yip, and Ho.[1] This effectively simulates an infinite tilt angle plane (an x-y plane) in the center of the model, sandwiched between (013) planes of atoms in roughly a bulk configuration. The kite-shaped structure outlined in the center boundary region represents the long-range periodicity of the boundary. The lighter-colored atoms are mobile in the dynamic portion of the simulation; the darker atoms are immobile. The dynamic region of the model contains 600 atoms and has dimensions as follows: $5a_0$ in the x direction, $(3\sqrt{10}/2)a_0$ in the y direction, and $(21/\sqrt{10})a_0$ in the z direction. The fixed walls contain enough (013) layers of atoms to extend beyond the cutoff length of the particular pair potential being used, so that a mobile atom near the fixed wall interacts with perfect bulk solid. Typically this requires ~ 300 fixed atoms, so that the total bicrystal model size is $N \cong 900$ atoms. In both the bicrystal and bulk model all three dimensions are ~ 20 Å in length, which was chosen so as to be at least 3 times longer than the cutoff length of any of the pair potentials.
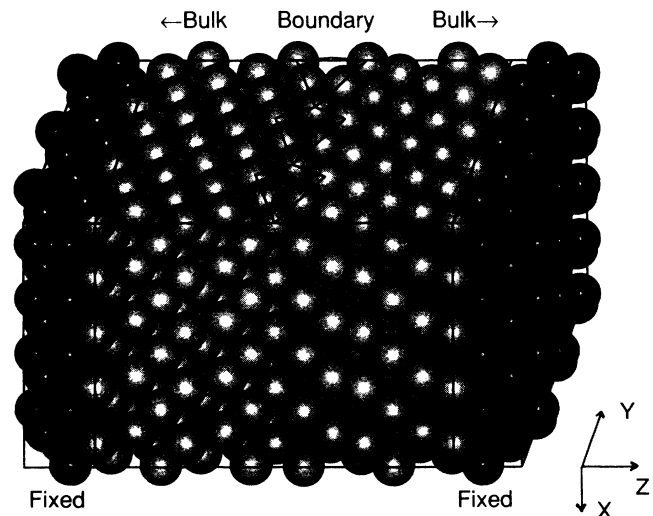

FIG. 1. Three-dimensional representation of a $\Sigma = 5$ (013) coincidence tilt boundary in a fcc lattice. The bicrystal model is periodic only in the x and y directions. The lighter-colored atoms move during the dynamic part of the simulation; the darker ones are held fixed.

Because the presence of the fixed walls of atoms is a nonphysical restriction, a few comments are in order. Their effect is to damp the motion of atoms near the walls. A method that avoids this is that of Broughton and Gilmer,[4] who simulated coincidence twin boundaries. The presence of a second boundary oriented opposite to the first means the ends of the simulation box are now of similar orientation and thus the box can be periodic in all three dimensions. We performed our simulations on such a model and found similar diffusion coefficients for the boundary regions as in our simpler bicrystal model. However, in the twin model the boundaries have a relatively low activation energy for migrating in the z direction, which makes it difficult to accumulate good statistics and calculate a consistent diffusion coefficient for grain-boundary atoms. In some cases the two boundaries would annihilate each other, leaving the entire model in a bulk configuration. Thus in the bicrystal model, the walls of fixed atoms, while nonphysical, have the beneficial effect of keeping the grain boundary centered where good statistics for the diffusion can be generated. A second type of border condition, used by Nguyen et al.,[5] involves replacing the fixed walls with duplicates of atoms from the dynamic region, so that each border atom moves in step with a dynamic companion atom. We did not implement this technique, but instead simulated the model with successively larger z dimensions while monitoring the motion of the grain-boundary atoms. The smallest z dimension was chosen (for speed of calculation) that did not constrain the atoms in the grain boundary.

To find the static 0-K structure for the bicrystal model, the ideal atom positions given by the CSL model must be relaxed so each atom feels no force. The forces between atoms are derived from the pair-potential approximation for the system's energy Φ, written as

$$\Phi = \sum_{i=1}^{N} \sum_{j>i} \phi(r_{ij}) , \qquad (1)$$

where ϕ is the energy of interaction between two atoms i and j separated by a distance r_{ij}, and the sum is over all pairwise interactions in the model. The energy was minimized using conjugate-gradient techniques, allowing the bicrystal to expand or contract in the z direction (perpendicular to the boundary) as well as allowing each atom to move relative to its neighbors. The amount of z-direction expansion which gave an energy minimum varied for the different potentials from $-0.026a_0$ to $0.225a_0$. In addition, a (013) plane of atoms at the boundary was removed to give a lower-energy state, as others[2] have noted is proper for the $\Sigma = 5$ fcc boundary.

The dynamic part of the simulation was performed for constant N, volume V, and energy E, consistent with the microcanonical ensemble. At time $t = 0$ each atom was given a random velocity consistent with a total system energy chosen so that the system would equilibrate at a desired temperature. The lattice was also expanded by an amount appropriate for that temperature and the linear thermal-expansion coefficient for Al ($\alpha = 25 \times 10^{-6}/K$), so that at each temperature the lattice spacing matched the experimental value for bulk Al. While this did not

keep the pressure constant across a wide temperature range for all the potentials, doing so in some cases would have required a nonlinear thermal-expansion coefficient. Also, the actual value of the calculated pressure seemed to be an artifact of the particular potential used, so that this method allowed more consistency in comparing results between potentials.

For computational speed, Newton's equations of motion for the system were integrated by the simple leap-frog method, using a time step equal to $\frac{1}{30}$ of the period T of highest-frequency atomic vibration as given by $T = h/k_B \Theta_D$, where h and k_B are the usual constants, and Θ_D is the Debye temperature for Al (428 K). This gives a time step of 3.74×10^{-15} sec. Typically, the simulation conserved energy to within 1% over 1000 time steps; the velocities were rescaled periodically by a small amount to keep the total energy exactly constant.

As the simulation progressed, the trajectory of each atom was generated. A sample set of trajectories for a (100) plane of the bicrystal model is shown in Fig. 2. While atoms away from the grain boundary primarily oscillate around their lattice sites, in the grain boundary atomic jumps to near-neighbor sites and in the $\pm x$ direction, as well as generalized diffusive motion, are evident. This motion allows the diffusion coefficient D in the two models to be calculated from the mean-square displacement of individual atoms by the equations

$$D = \frac{\sum_{i=1}^{N} (x_i - x_{i_0})^2 + (y_i - y_{i_0})^2}{4Nt} \quad \text{(bicrystal model)} ,$$

$$D = \frac{\sum_{i=1}^{N} (x_i - x_{i_0})^2 + (y_i - y_{i_0})^2 + (z_i - z_{i_0})^2}{6Nt}$$
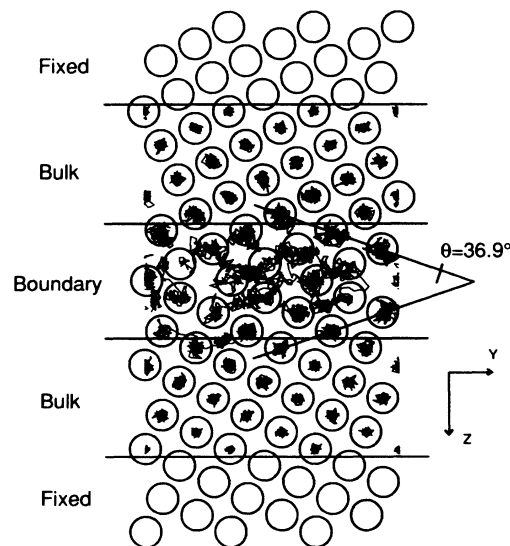
(bulk model) ,

(2)

FIG. 2. Atom trajectories for one (yz) plane (see Fig. 1) of the Al grain boundary simulated for ~ 11 psec (3000 time steps) at 800 K. The circles represent initial $t = 0$ positions of the atoms; the lines are their trajectories in time. Most of the atomic diffusion occurs in the center grain-boundary region.

where t is the time elapsed in the simulation, $(x_{i_0}, y_{i_0}, z_{i_0})$ is the original $t = 0$ position of atom i, and (x_i, y_i, z_i) is its current position. In the limit of long simulation times, the slope of the mean-square displacement-versus-time data should be constant for a region undergoing random-walk diffusion; hence the diffusion coefficient is defined for the region. For the bulk model, statistics could be accumulated for all $N = 500$ atoms. For the bicrystal model the boundary was defined as being seven (013) planes in width ($\sim 9 \text{Å}$), which encompassed $N = 180$ atoms. Only two of the three dimensions (x and y) were included in the bicrystal part of Eq. (2) since diffusion perpendicular to the boundary was typically 50% less than in the plane of the boundary. Simulation runs were also limited to between 25 000 and 50 000 time steps (~ 100 psec), so that mixing of grain-boundary atoms with atoms from the bulk regions of the model was negligible. This, coupled with the exclusion of z-direction motion in Eq. (2) and the lack of z-direction migration of the boundary itself (as noted previously), allowed a consistent diffusion coefficient to be calculated for grain-boundary atoms. An example of mean-square displacement data for the bicrystal model is shown in Fig. 3(a).

It should be noted that D in an asymmetric region like a grain boundary is actually a tensor quantity. Equation (2) for the bicrystal is an average over two of the tensor components. In contrast to the bicrystal simulation of Kwok, et al. of a $\Sigma = 5$ α-Fe tilt boundary,[1] we did not

observe diffusion in the boundary plane to be greater parallel to the tilt axis than perpendicular to it. This was true for all of the potentials studied. This may be because of differences between fcc and bcc diffusion, or because molecular-dynamics simulation times are not long enough to distinguish between the various directions of diffusion. However, runs as long as those in Ref. 1 were performed (up to 400 psec) without a statistically significant difference being detected.

The activation energy Q for atomic motion in the boundary region and in bulk was measured by calculating D at various temperatures and fitting to the general diffusion relation

$$D = D_0 \exp\left[-\frac{Q}{k_B T}\right], \tag{3}$$

which yields Q and the prefactor D_0. If a vacancy mechanism for the diffusive motion is assumed, then Q is the sum of a migration energy Q_m and a vacancy-formation energy Q_f. In an attempt to extract the Q_m portion of the activation energy, the jump frequency for atomic hopping as a function of temperature was monitored. This requires defining what is meant by a "jump" from one lattice site to another. We proceeded analogously to Kwok et al.[1] by assigning a spherical volume to each lattice site, equal in diameter to $\frac{9}{10}$ the nearest-neighbor distance in the bulk lattice. As the simulation progressed, an atom was flagged when it moved from its current sphere to a second one on another lattice site. If it stayed inside the new sphere for two vibrational periods (60 time steps) or moved on to a third sphere, it was assumed to have "jumped" to the second site. This could only happen when the new site was unoccupied (i.e., vacancy diffusion) or by a kind of cooperative mechanism where several atoms changed lattice sites more or less simultaneously. By counting the jumps and vacancies that were created, the quantity Γ, the average jump frequency per vacancy, was calculated as a function of temperature. The relation

$$\Gamma = \Gamma_0 \exp\left[-\frac{Q_m}{k_B T}\right] \tag{4}$$

allows the migration energy Q_m and prefactor Γ_0 (which is related to an attempt frequency) to be extracted. The difficulty with this method is that Γ must be calculated as an average over all vacancy trajectories active in the model at a particular time. At lower temperatures ($\sim \frac{1}{2}$ the melting temperature T_m) only one or two vacancies were typically created, and this is not difficult. However, at temperatures nearer T_m the grain boundary becomes very disordered (a more liquidlike diffusion begins to take place), and calculating the vacancy concentration becomes ambiguous.

A final calculation that proved useful was to monitor the atomic disordering by calculating the structure or melting factor S at different locations within the bulk and bicrystal models. This is given by

$$S(\mathbf{K}, z) = \left\langle \frac{1}{N_z^2} \left| \sum_{j=1}^{N_z} \exp(i\mathbf{K} \cdot \mathbf{r}_j) \right|^2 \right\rangle, \tag{5}$$
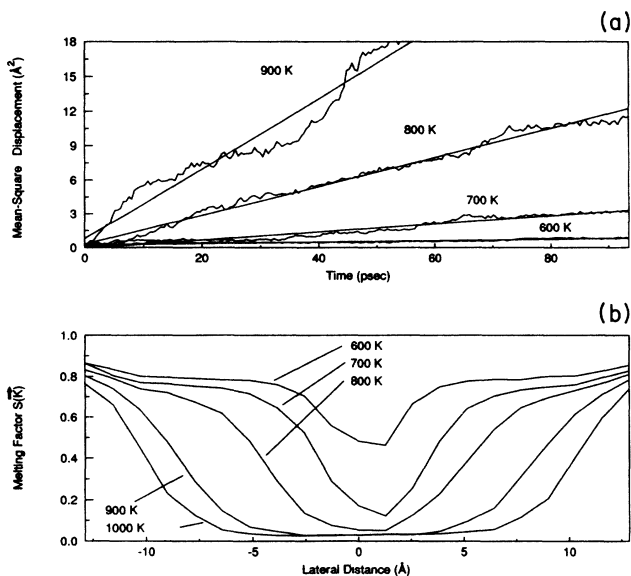

FIG. 3. (a) Mean-square displacement of atoms in the grain-boundary region of the bicrystal model vs simulation time at several temperatures. The linear data mean random-walk diffusion is taking place; the slopes of the straight-line fits are proportional to the diffusion coefficient for the region. (b) Melting factor $S(\mathbf{K})$ calculated across the z direction of the bicrystal model (see Fig. 1) for the same set of temperatures as in (a). The "dip" in the center of each curve is increased grain-boundary disordering as the temperature rises.

where **K** is the reciprocal-lattice vector $(4\pi/a_0)(1,0,0)$, N_z is the number of atoms in a thin (xy) planar slab of the model at a given z position, $\mathbf{r}_j$ is the position of atom j, and $\langle\ \rangle$ denotes a time average. The value of S ranges from 1.0 for a perfectly ordered solid to 0.0 for a perfectly disordered or melted one. An example of these data for different temperatures in the bicrystal model is shown in Fig. 3(b), calculated from left to right across the grain boundary (so that the boundary is in the center of the plot). The curves for successively higher temperatures show increased disordering (and finally melting) in the boundary region, while the adjacent bulk regions show only a slight decrease in S, consistent with an increased amplitude of vibration by those atoms around their lattice sites (but no melting). At lower temperatures the only effect of the fixed walls is a slight upturn of the data at the ends of each curve, meaning the amplitude of vibration is less for atoms nearest the wall, as anticipated. At higher temperatures the width of the melted region is restricted by the presence of the fixed walls; however, as mentioned previously, motion in the grain boundary itself is not restricted.

III. RESULTS AND ANALYSIS

There are a wide variety of Al interatomic pair potentials available in the literature. For this study one pseudopotential and three empirical potentials were chosen as representative of the different methods typically employed in deriving a pair-potential function. They are plotted in Fig. 4 as potential energy ϕ for two atoms separated by a distance r.

The first potential, Al1, is the pseudopotential of Dagens and Rasolt.[15] Although it extends indefinitely, for computational purposes it was truncated where it crosses the axis at a distance $r = 4.832$ Å. The second potential, Al2, is due to Esterling and Swaroop,[16] who fitted piecewise fourth-order polynomials to experimental Al phonon spectra. The potential Al3 is the standard semiempirical Morse potential for Al, with parameters chosen so that it gives the correct experimental compres-
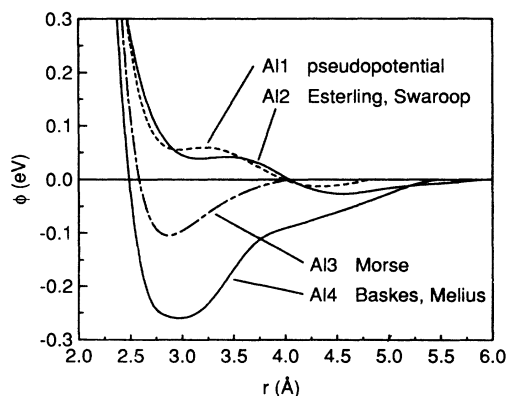
sibility factor, energy of vacancy formation, and lattice constant for the bulk material. Parameter values for Al derived by Cotteril and Doyama[17] were used for a potential that extends to the second-nearest-neighbor distance (4.04 Å) in the Al lattice. It was then truncated and shifted so that it went to zero at that distance. The final potential, Al4, due to Baskes and Melius,[18] is a piecewise cubic spline fit to various experimentally determined bulk properties, including the energies of vacancy formation and migration, the elastic constants, and the stacking-fault energy.

All the potential functions, when applied to a group of atoms, include a volume-dependent term. In constant NVE molecular dynamics this term is ignored since the volume is held fixed. However, we performed an analysis due to Najafabadi and Kalonji[19] which involves calculating the response of a bulk crystal to tensile stress applied along one crystal axis. It was found that of the four potentials, only the More potential, Al3, was in equilibrium (zero stress and an energy minimum) at the correct lattice spacing of 4.04 Å. This means the other three potentials require the volume-dependent term to be in static equilibrium with the proper fcc lattice as the minimum-energy configuration. This suggests caution in interpreting simulation results across a range of temperatures (which requires changing the system volume); however, this is a problem inherent in the pair-potential approach.

From Fig. 4 it is also clear that while all four potentials are similar in general shape, there is considerable variation in the position and depth of the primary potential well near the nearest-neighbor distance (2.86 Å). This is particularly evident when the interatomic force $F(r) = -(d/dr)\phi(r)$ is calculated. The four Al potentials give widely differing force interactions due to the many inflection points and local minima some of them contain. Thus one would expect there might be a significant dependence of the dynamic properties of simulated Al on these differences in the force functions.

The diffusion data resulting from the simulation for both the bicrystal and bulk model over a range of temperatures for each potential are shown in Fig. 5 plotted versus reciprocal temperature and normalized by the experimental melting temperature of Al (930 K). The open symbols are grain-boundary diffusion data for each of the four potentials; the corresponding solid symbols are for bulk. Typically, two runs of 25 000 time steps with different initial conditions were performed at each temperature. This gave a statistical variation of roughly a factor of 2 in the diffusion coefficient at lower temperatures due to the random-walk nature of the diffusion. Longer runs (100 000+) of time steps were no better in this respect, so multiple short runs were a more efficient means of generating good data. Each set of data in Fig. 5 is fitted by a straight line so that D_0 and Q can be extracted using Eq. (3). These values are listed in Table I, as are results for Q_m as calculated by Eq. (4) and the simulation data for atom-hop frequencies. In all but one case, $Q_m < Q$ as expected. The one exception (bulk Al3) is due to the extraction of both Q and Q_m from the very limited amount of bulk diffusion the Al3 potential allows, even for runs at temperatures above 930 K (as seen in Fig. 5).

FIG. 4. Interatomic pair potentials for Al. References are given in the text. The nearest-neighbor distance in the fcc Al lattice is 2.86 Å.
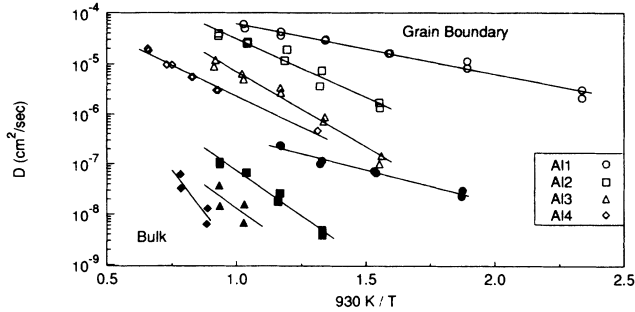
FIG. 5. Simulated diffusion data for the four potentials of Fig. 4 plotted vs reciprocal temperature. Open symbols are for grain-boundary diffusion in the $\Sigma=5$ bicrystal model; the corresponding solid symbols are for diffusion in the bulk model.

For runs of 25 000 time steps both the Al3 and Al4 potentials allowed only one to four diffusive hops at the lower temperatures and about ten at the higher. In contrast, runs for the Al1 and Al2 potentials in bulk produced more than 50 hops at the same temperatures, and runs for the grain-boundary model typically produced hundreds or even thousands of hops. Hence, the Q and Q_m values for bulk Al3 and Al4 are coarser estimates than the other activation energies in the table.

Several other comments concerning the data of Fig. 5 and Table I are in order. First, Gjostein[20] and Hwang and Balluffi[21] give compilations of experimental diffusion data in grain boundary and bulk for many fcc metals plotted versus the homologous temperature T_m/T. At T_m for all fcc metals, D is $\sim 1.0\times 10^{-4}$ cm²/sec for grain-boundary diffusion and $\sim 1.0\times 10^{-8}$ cm²/sec for bulk diffusion. The activation energy Q for Al from these two references, as well as electromigration experiments performed on pure-Al thin films,[22] is 0.4–0.7 eV for grain-boundary diffusion and 1.2–1.7 eV for bulk. However, the spread in data in the Hwang-Balluffi compilation of grain-boundary data is such that at a given temperature there is at least a (2–3)-order-of-magnitude uncertainty in D. Comparing Fig. 5 and Table I to these numbers shows that much of the simulation data is of the right order of magnitude near the melting temperature, but that the activation energies are somewhat low. One reason for this, particularly for the bulk data, is that at the beginning of each simulation run one atom was re-

moved from the model (bicrystal and bulk) so as to provide an initial vacancy for diffusion to begin. In the bicrystal model, runs with and without this initial vacancy gave very similar diffusion results. This was true for the bulk model at temperatures near T_m, but for $T < \sim \frac{3}{4}T_m$, atoms in the bulk model without the initial vacancy would not diffuse (i.e., there was not sufficient energy to create the first vacancy). This means that the bulk data overestimate the true diffusion rate, at least at lower temperatures, and hence the extracted activation energy is also lower. This is somewhat fortuitous in that the lower level of detectability of the simulation is $D \cong 3.0\times 10^{-9}$ cm²/sec [one nearest-neighbor hop in 25 000 time steps for an ($N=500$)-atom model], but to be consistent with the other diffusion data, this overestimation is not corrected for in the raw data of Fig. 5.

The following correlation between the data of Fig. 5 and the pair potentials of Fig. 4 can also be noted. Potential Al1 has the shallowest potential well at the nearest-neighbor distance (2.86 Å) and also the fastest diffusion rate at a given temperature. Conversely, Al4 has the deepest well and slowest diffusion rate. This matches the intuitive model of an atom hop to an adjacent vacancy being moderated by the height of the potential barrier created primarily by its near neighbors. To test the idea that the inner repulsive part of the potential is the most critical, the bicrystal model was simulated using Al1 (the pseudopotential) with several cutoff values so that the potential ranged in extent from 3.99 to 6.65 Å. Almost no variation in the diffusion coefficient was found, meaning the "tail" of the potential has little effect on the diffusion to first order.

The analysis can be made more quantitative in the following way. We observed that all four potentials gave similar melting-factor, $S(K)$, data for disorder in the grain-boundary region over a range of temperatures, as in Fig. 3(b). However, the temperature at which disordering took place varied widely between potentials. Furthermore, if "melting" of the grain-boundary region was defined as an $S(K)$ value of 0.1 [a temperature of ~ 800 K in Fig. 3(b)], then all the potentials showed similar grain-boundary diffusion rates at their respective "melt" temperatures. This suggested that rescaling the diffusion data by a bulk melting temperature unique to each potential would reduce the spread of data in Fig. 5.

To estimate the bulk T_m induced by each pair potential, $S(K)$ from Eq. (5) was calculated for the bulk model.

TABLE I. Diffusion prefactors D_0 and activation energies Q for each of the four Al potentials extracted from the data of Fig. 5 for both grain-boundary and bulk diffusion. The method for estimating the migration energies Q_m and bulk melting temperatures T_m is discussed in the text.

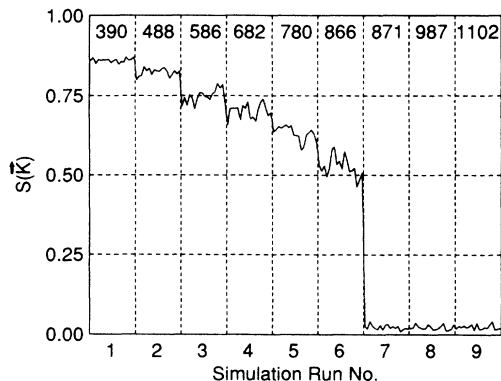| Potential	Grain boundary			Bulk			
	D_0 (cm²/sec)	Q (eV)	Q_m (eV)	D_0 (cm²/sec)	Q (eV)	Q_m (eV)	T_m (K)
Al1	5.98×10^{-4}	0.183	0.088	6.55×10^{-6}	0.238	0.229	900
Al2	6.07×10^{-3}	0.424	0.251	2.95×10^{-4}	0.664	0.552	1200
Al3	7.07×10^{-3}	0.554	0.229	6.81×10^{-5}	0.685	1.06	1600
Al4	6.64×10^{-4}	0.455	0.239	8.65×10^{-3}	1.24	1.01	1700

FIG. 6. Melting factor $S(\mathrm{K})$ for nine simulation runs in the bulk model for the pseudopotential of Fig. 4. Each run began at an incrementally higher energy; the equilibrated temperature for each (in K) is listed at the top of the plot. This potential gives a disordering or melting at ~ 870 K (experimental T_m for Al is 930 K). The temperature plateau between runs 6 and 7 indicates energy has gone into disordering the lattice (increased entropy).

Figure 6 is an example for the pseudopotential Al1. Nine runs of the simulation were made at incrementally higher initial energies as shown along the x axis. During each run the model was allowed to equilibrate for several thousand time steps at the temperature shown at the top of each vertical segment. Within each segment, the melting factor across one dimension of the simulation cube is plotted. The trend of the data is clear: as the temperature increases, so does disorder, until at a temperature of $T_m \cong 870$ K there is a sharp transition to a disordered state (between runs 6 and 7). Although the total energy is different for the two runs, the temperature is almost equal, which means the added energy went into disordering the bulk solid (a phase transition). This is, of course, not the best way to measure a melting temperature, since
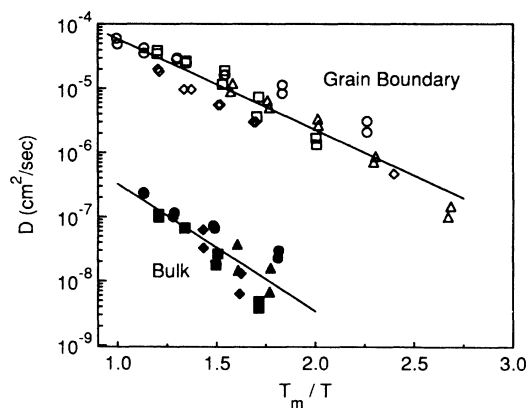

FIG. 7. Simulated diffusion data of Fig. 5 replotted vs reciprocal temperature, but normalized by the T_m appropriate to each potential (see Table I). The meaning of the symbols is the same as in Fig. 5. Within an order-of-magnitude variation, all grain-boundary and bulk diffusion values now lie on the same lines.

the constant-volume constraint surely affects the result, and superheating of the crystal structure (past the real melting point of the solid) is known to be a problem for molecular dynamics. However, the simulation was performed for larger bulk models (up to 1372 atoms) with the same results for T_m, so that it is at least a rough estimate of the melting temperature consistent with the NVE ensemble. Rounded values of T_m thus obtained for the four Al potentials are listed in Table I and range from close to the experimental value of 930 K for Al1 to 1700 K for Al4.

Using these values, the diffusion data of Fig. 5 were replotted versus the T_m/T ratio appropriate for each potential. The results are shown in Fig. 7. The variation between data for the different potentials is now less than an order of magnitude, as compared to the 2–3 orders of magnitude before. The equation for the fitted line for the grain-boundary diffusion is $D = D_0^* \exp[-Q^*(T_m/T)]$, where $D_0^* = 1.54 \times 10^{-3}$ cm^2/sec and $Q^* = 3.26$. The bulk data are fitted by the same equation with $D_0^* = 3.11 \times 10^{-5}$ cm^2/sec and $Q^* = 4.56$.

IV. POTENTIAL PARAMETERS AND CONCLUSIONS

To test the generality of the preceding analysis, the effect of adapting the shape of the Al3 Morse potential was simulated. The equation for the Morse potential is

$$\phi(r) = \phi_0(e^{-2\alpha(r-r_0)} - 2e^{-\alpha(r-r_0)}) \, , \qquad (6)$$

where the three free parameters in the potential are ϕ_0, which determines the depth of the potential well; r_0, which sets its position; and α, which determines its steepness. By adjusting any or all of the parameters, the shape of the potential function and hence the interaction force of an atom with its near neighbors can be tailored. To isolate their effects, each parameter was varied over a small range of values centered on $\phi_0 = 0.12$ eV, $r_0 = 2.86$ Å, and $\alpha = 2.35$ Å^{-1} as used in the Al3 formulation of the Morse potential.[17] Each adapted potential was used in the bicrystal model to calculate a grain-boundary diffusion coefficient at 900 K. The results are shown in Fig. 8 as three curves, one for each of the parameters. The units along the x axis signify that each parameter is varying linearly between the values shown at each end of the curves. The point common to all three curves is for parameter values of the Al3 potential. We note that the general shape of the curves matches one's intuition regarding the effect of Eq. (6) on atomic motion. For example, a linear change in ϕ_0 changes the potential barrier height linearly. Since the atoms are thermally activated to cross the barrier, a linearly increasing barrier height implies an exponential falloff in the diffusion. Hence the ϕ_0 curve in Fig. 8 is linear on the logarithmic plot. Similarly, since r_0 appears in the exponent of Eq. (6), a linear increase in r_0 gives an exponential increase in the barrier height. This should give a faster-than-linear falloff in the diffusion rate for increasing r_0, as is indeed the case in Fig. 8. The same analysis should hold for α since it also appears in the exponent of Eq. (6). However, the α curve
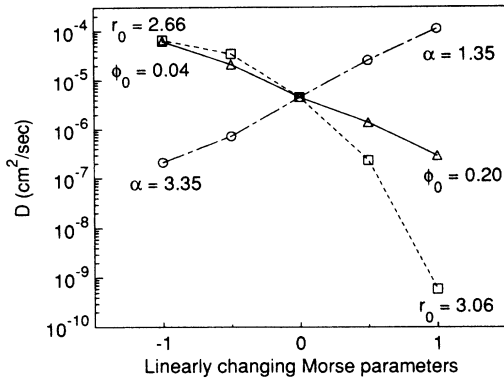
FIG. 8. Grain-boundary diffusion data at 900 K for a Morse potential using different values of the potential parameters r_0 (dashed curve), ϕ_0 (solid curve), and α (dashed-dotted curve). The point common to all three curves is for $r_0 = 2.86$ Å, $\phi_0 = 0.12$ eV, and $\alpha = 2.35$ Å^{-1} (the standard values for the Al3 Morse potential truncated at the second-nearest-neighbor distance).

shows only a linear increase in diffusion for decreasing α.

Bulk melting temperatures for each of the 12 adapted Morse potentials were estimated from the bulk $S(K)$ data as in the preceding section. As before, each potential showed a melting transition at a specific T_m, which, for the 12 potentials, ranged from 500 to 3000 K. When the diffusion data of Fig. 8 were plotted versus a normalized T_m/T, all 12 values fell nearly perfectly on the grain-boundary line of Fig. 7, with even less spread than the diffusion data of the original four Al potentials. This is evidence that the curves of Fig. 7 are, in a sense, universal relations representing normalized diffusion for any potential that can be constructed, physical or not, for the Al bicrystal and bulk models.

To carry the analysis one step further, a relation between potential barrier height and T_m was sought that would enable the diffusion properties of a potential to be predicted easily. An analog is the empirical relation noted by Shewmon[23] between activation energy and melting temperature, which holds for many metals and is of the form $Q/T_m = K$, with K a constant. The barrier height in the bulk model for an atom to jump to an adjacent vacancy is the difference between its energy on its lattice site and that on the saddle point of the barrier (midway between the two lattice sites). We first calculated these energies by placing atom i at one of these locations (a lattice site adjacent to a vacancy or on the saddle point) and relaxing the positions of the remaining atoms around it with a conjugate-gradients algorithm to minimize the total energy of the model. The height of the energy barrier was then calculated by the sum of interactions $\sum_{j \neq i} \phi(r_{ij})$ for atom i with all other atoms in the model. When calculated for several different potentials, this gave a roughly linear relation between barrier height and T_m. However, surprisingly, a much better correlation was achieved for the same calculation done without relaxing the surrounding atoms (and has the advantage of being simpler

to implement as well). First, the bulk lattice was expanded by a factor $1 + \alpha T_m$, where α is the thermal-expansion coefficient for Al, the same as when the molecular-dynamics simulation is performed. Then the sum of $\phi(r_{ij})$ for atom i interacting with its neighbors (all on their unrelaxed perfect lattice sites) is done for atom i at the saddle point and its original lattice site (adjacent to a nearest-neighbor vacancy). The difference between the two energies is Q_{SB}, a static barrier height of sorts. The results of this calculation for each of the four original Al potentials and the 12 adapted Morse potentials versus their respective melting temperatures T_m are shown in Fig. 9. It can be seen that within an error of ± 200 K all the values fall on the same line, which, by analogy with the Shewmon relation, is given by the equation $T_m = (1918 \text{ K/eV})Q_{SB} - (102.5 \text{ K})$. We believe this is again a universal relation that holds for all Al potentials. Its significance is that it that it can be used to correlate simulation results between two different potentials or, indeed, to predict simulation results for any potential in the following way. Given a particular pair-potential function, the barrier calculation outlined above can be done over a range of lattice expansions (which correspond to different temperatures). This generates a curve similar to the dotted line in Fig. 9. This particular line is for the Al3 Morse potential. The point where the dotted line crosses the solid line gives a rough estimate of the melting temperature that potential will induce in a bulk sample (within the NVE constraints mentioned previously). Once T_m is known, the diffusion at any temperature in the grain boundary or bulk can be estimated from the curves in Fig. 7. Thus, a simple static calculation of the barrier height Q_{SB} yields dynamic diffusion results without the need to perform the more time-consuming dynamic simulation. Furthermore, although the work presented here has all been for Al potentials, it can easily be extended to other fcc metals since the only quantity
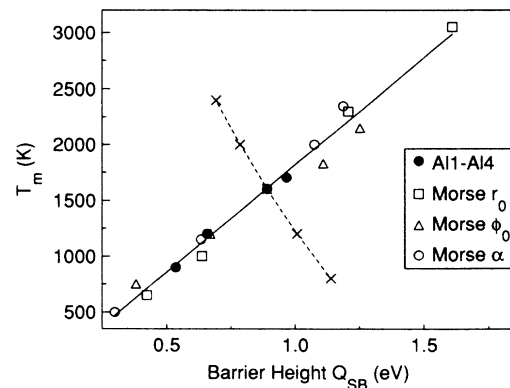

FIG. 9. Melting temperature plotted vs barrier height for bulk vacancy diffusion (calculation explained in the text) for each of the four Al potentials of Fig. 4 and for the 12 adapted Morse potentials of Fig. 8. The significance of the dotted line is discussed in the text.

relative to the pair potential appearing in the molecular-dynamics equations for the atomic motion is a factor of F/m, F being the interatomic force $-d\phi/dr$ and m the atomic mass of the simulated material. If the interatomic force derived from any potential is written in reduced units of eV/a_0 (where a_0 is the lattice constant of the metal) and scaled by the mass m, a homologous Al potential can be derived. The above method would then predict the new potential's diffusive properties. Hence, grain-boundary and bulk diffusion rates can be predicted for any fcc material and any pair potential.

In summary, idealized models of a $\Sigma=5$ (013) tilt boundary bicrystal and a bulk solid have been used to simulate diffusion at grain boundaries and in bulk via the techniques of molecular dynamics. We have shown the choice of interatomic pair potential to be a critical factor in determining the mobility of diffusing atoms. In particular, diffusion coefficients can vary by 3 orders of magnitude for simulations at the same temperature with different potentials. This is because the shape of the principal potential well differs widely for different pair potentials, and its depth, width, and position affect the ability of an atom to diffuse past its neighbors.

Using the structure factor S to determine the melting temperature T_m that a potential induces in a bulk model correlates the results of different potentials. Just as diffusion rates and other dynamic properties of most bulk solids scale with their relative melting temperatures, so too does each potential's respective T_m normalize the diffusion results. This was found to be true for several Al potentials from the literature as well as for a set of adapted Morse potentials. By calculating the height of the potential barrier that each pair potential creates for a diffusing atom in a static bulk model, a universal relation between T_m and the barrier height Q_{SB} for each potential was found. This enables the diffusive properties of any potential for any fcc material to be predicted without resorting to a time-consuming full-scale molecular-dynamics simulation. Because the diffusion of atoms underlies many dynamic effects, such as crack formation and propagation and electromigration, it should be possible to extrapolate the effect of the choice of pair potential on those kinds of simulation as well. We are not certain if this same relation between Q_{SB} and T_m applies to bcc metals since the diffusion mechanisms may well be different. Also, we have only presented results for a $\Sigma=5$ boundary; we are currently performing dynamic simula-

tion of diffusion in tilt boundaries of varying geometry to see if similar relations can be derived.

Finally, as to the question of which pair potential is "best" in the dynamic sense, no easy answer can be given. None of the four potentials studied here gives totally satisfactory diffusion rates across a wide range of temperatures in grain boundary and bulk when compared to experiment. Our results indicate that it is perhaps more important to be able to compare results between different pair potentials than to interpret the magnitude of a particular simulation's result, since that can be an artifact of the pair potential used. (A side benefit of this fact is that, in practice, it should be possible to use very-short-range potentials that induce more diffusion to speed up lengthy dynamic calculations, and then map the results to more realistic potentials). This is likely a flaw inherent in the pair-potential approximation and the constraints of NVE molecular dynamics. Recent work by Adams et al.[24] using the embedded-atom method in a molecular-statics calculation to calculate activation energies, and thus deduce bulk diffusion rates for a variety of transition metals, gave good results when compared to experiment. Since, as noted in the Introduction, the EAM has advantages over pair potentials in describing grain-boundary interactions, it can be hoped that full EAM dynamic simulations of boundary diffusion will yield more accurate results than seem possible within the pair-potential approximation.

*Present address: Division 1424, Sandia National Laboratories, Albuquerque, NM 87185.

[1]T. Kwok, P. S. Ho, and S. Yip, Phys. Rev. B **29**, 5354 (1984); **29**, 5363 (1984).

[2]T. Kwok, P. S. Ho, and S. Yip, Surf. Sci. **44**, 144 (1981).

[3]G. Ciccotti, M. Guillope, and V. Pontikis, Phys. Rev. B **27**, 5576 (1983).

[4]J. Q. Broughton and G. H. Gilmer, Phys. Rev. Lett. **56**, 2692 (1986).

[5]T. Nguyen, P. S. Ho, T. Kwok, C. Nitta, and S. Yip, Phys. Rev. Lett. **57**, 1919 (1986).

[6]G. H. Bishop, Jr., R. J. Harrison, T. Kwok, and S. Yip, J. Appl. Phys. **53**, 5596 (1982); **53**, 5609 (1982).

[7]R. Najafabadi and G. Kalonji, Scr. Metall. **22**, 1049 (1988).

[8]B. de Celis, A. S. Argon, and S. Yip, J. Appl. Phys. **54**, 4864 (1983).

[9]M. I. Baskes, S. M. Foiles, and M. S. Daw, J. Phys. (Paris) Colloq. **49**, C5-483 (1988).

[10]D. Wolf, Acta Metall. **32**, 245 (1984).

[11]P. D. Bristowe and S. L. Sass, Acta Metall. **28**, 575 (1980).

[12]V. Pontikis, J. Phys. (Paris) Colloq. **49**, C5-327 (1988).

[13]M. S. Daw and M. I. Baskes, Phys. Rev. B **29**, 6443 (1984).

[14]S. M. Foiles, Phys. Rev. B **32**, 3409 (1985).

[15]L. Dagens, M. Rasolt, and R. Taylor, Phys. Rev. B **11**, 2726 (1975).

[16]D. M. Esterling and A. Swaroop, Phys. Status Solidi B **96**, 401

(1979).

[17]R. J. M. Cotterill and M. Doyama, in *Lattice Defects and Their Interactions*, edited by R. Hasiguti (Gordon and Breach, New York, 1967), p. 1.

[18]M. I. Baskes and C. F. Melius, Phys. Rev. B **20**, 3197 (1979).

[19]R. Najafabadi and G. Kalonji, Acta Metall. **36**, 917 (1988).

[20]N. A. Gjostein, in *Diffusion* (American Society for Metals, Metals Park, OH, 1973), p. 241.

[21]J. C. M. Hwang and R. W. Balluffi, Scr. Metall. **12**, 709 (1978). See also G. Martin and B. Perraillon, in *Grain Boundary Structure and Kinetics*, edited by R. W. Baluffi (American Society for Metals, Metals Park, OH, 1979), p. 239, who extracted the self-diffusion portion of this data.

[22]H. U. Schreiber and B. Grabe, Solid-State Electron. **24**, 1135 (1981).

[23]P. G. Shewmon, *Diffusion in Solids* (Williams, Jenks, OK, 1983), p. 65.

[24]J. B. Adams, S. M. Foiles, and W. G. Wolfer, J. Mater. Res. **4**, 102 (1989).
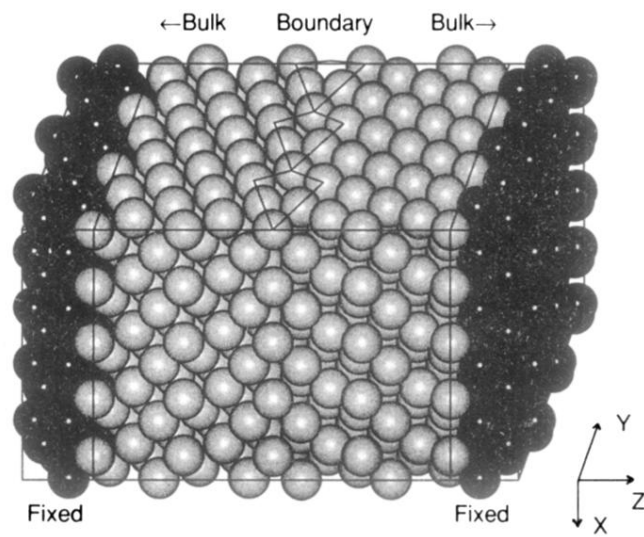
FIG. 1. Three-dimensional representation of a $\Sigma = 5$ (013) coincidence tilt boundary in a fcc lattice. The bicrystal model is periodic only in the x and y directions. The lighter-colored atoms move during the dynamic part of the simulation; the darker ones are held fixed.